

of residual (and hence hardly measurable) e^+e^- pairs at present and near-future laser installations.

Our paper is organized as follows. In section II, we present a formula for calculating the photon spectrum which arises, in first-order perturbation theory, as a consequence of Schwinger pair production. Based on such an approach to the time-integrated final-stage photon yield (the ‘‘afterglow’’) we provide in section III numerical evaluations for the Sauter pulse and a periodic pulse modulated by a time-limited envelope as important examples of field configurations, which have been also employed formerly in studying the plain Schwinger pair production. Here, we exemplify furthermore that the superposition of external fields with different time scales can result in order-of-magnitude amplifications of the emergent photon yield, similarly to the dynamically assisted Schwinger process. Our summary can be found in section IV. This main body of the paper uncovers the phenomenological aspects of our approach, up to an estimate of an ELI-NP-related prediction. All formal aspects of our approach are relegated to the appendices. Appendix A spells out in detail the foundations of our photon spectrum formula by exploiting suitable transits between Heisenberg picture and interaction picture to arrive at a solution to the photon wave equation and its relation to the fermion dynamics. Appendix B discusses the soft-photon spectrum and recalls the Bogoliubov transformation which is needed to make relevant formulas for fermion dynamics explicitly.

II. A FORMULA FOR THE PHOTON SPECTRUM

The impact of an external electric field on the quantum vacuum consists in inducing a vacuum current which in turn is a source of real-photon fluctuations. In the QED sector, the remainder of the vacuum current is a finite – and in general non-trivial – e^+e^- pair distribution, referring to the Schwinger process. We calculate the spectrum of emerging photons by solving the quantized Maxwell wave equation in first-order perturbation theory as

$$f_\gamma(\mathbf{k}) = \frac{e^2}{(2\pi)^6} \frac{1}{2\omega} \int d^3p \sum_{\lambda,r,s} |\epsilon_\lambda^\mu(\mathbf{k}) C_{rs\mu}(\mathbf{p}, \mathbf{k})|^2, \quad (1)$$

$$C_{rs\mu}(\mathbf{p}, \mathbf{k}) = \lim_{\varepsilon \rightarrow 0} \int_{-\infty}^{\infty} dt f_\varepsilon(t) \times \bar{v}_r(t, -\mathbf{p}) \gamma_\mu u_s(t, \mathbf{p} - \mathbf{k}) e^{-i\omega t} \quad (2)$$

highlighting the time-asymptotic photon yield and valid for a spatially homogeneous system. The photons propagate on the light cone, i.e. the frequency ω and wave three-vector \mathbf{k} are related by $\omega^2 - \mathbf{k}^2 = 0$ and their polarization four-vector ϵ_λ is orthogonal to the wave four-vector; $\lambda = 1, 2$ counts the polarization states. $f_\varepsilon = e^{-\varepsilon|t|}$ is an adiabatic switch-on/switch-off function of the external field, and \bar{v}_r and u_r are the time dependent Dirac

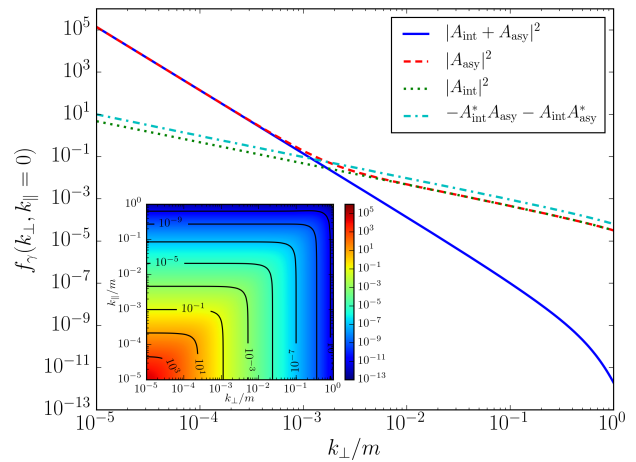


Figure 1. Asymptotic phase-space distribution $f_\gamma(\mathbf{k})$ displayed as a function of k_\perp at $k_\parallel = 0$ for the Sauter pulse with $E_0 = 0.2E_c$ and $\tau = 2/m$. Solid blue curve: full result; dashed red curve: contribution from the asymptotic time integral in (2) with $A_{\text{asy}} \propto (\int_{-\infty}^{-t_m} + \int_{t_m}^{\infty}) dt$; dotted green curve: contribution from the intermediate time integral $A_{\text{int}} \propto \int_{-t_m}^{t_m} dt$; dash-dotted cyan curve: the interference term of A_{asy} and A_{int} ; $A_{\text{asy,int}}$ are insensitive to variations of the matching time around $t_m = 20\tau$. The inset exhibits the contour plot of the phase-space distribution $f_\gamma(k_\perp, k_\parallel)$.

wave functions in that field. The details of formal operations to arrive at (1,2) are spelled out in Appendix A. Equations (1,2) allow for the first time a systematic study of the photon emission accompanying the Schwinger process. For instance, one can show (see Appendix B) that the soft photons are insensitive to details of the transient Fermion dynamics encoded in u_r and v_r , instead they reflect essentially the difference of *in*- and *out*-vacua. In contrast, the hard photons do resolve the actual background field dynamics, albeit in a time-integrated manner. Here, we meet severe interferences of the various contributions to the time integral in (2). In lacking analytical expressions for $\omega \gg m$ we resort to numerical solutions pointing to an exponential shape.

III. NUMERICAL RESULTS

1. Sauter pulse

The Sauter pulse with electric field $E(t) = E_0/\cosh^2(t/\tau)$ and potential $A(t) = E_0\tau(1 + \tanh(t/\tau))$ is an often used external field model which has an analytical solution of the time evolution of the e^+e^- pair density $N_{e^+e^-}(t)$ [12]; for $\tau > 50/m$ it recovers the seminal Schwinger result. Even if only $N_{e^+e^-}(t \rightarrow \pm\infty)$ has a sensible interpretation in terms of *in* and *out* asymptotic particle and anti-particle states, a curious fact is that the mode occupation in an adiabatic basis displays $N_{e^+e^-}(t \approx 0) \gg N_{e^+e^-}(t \rightarrow \infty)$ for deep-subcritical fields $E_0 \ll E_c$ [25, 26]. Our main result (1,2) does not

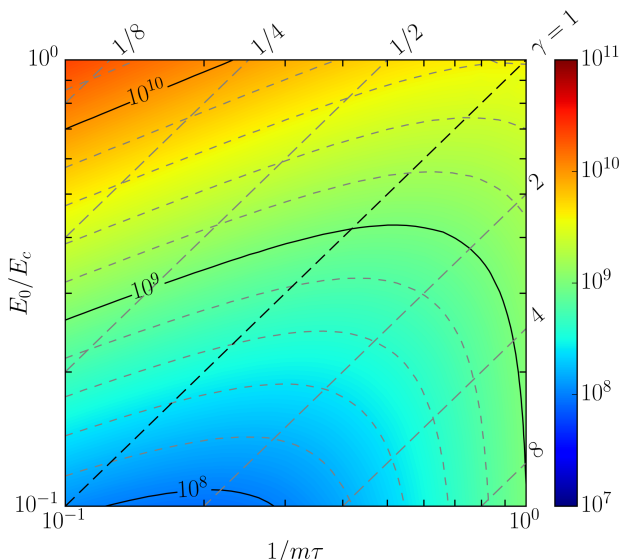


Figure 2. Contour plot of the asymptotic photon phase-space occupancy $f_\gamma(k_\perp = \omega, k_\parallel = 0)$ for $\omega = 10^{-5}m$ normalized to the asymptotic e^+e^- phase-space occupancy $f_{e^+e^-} = d^6 N_{e^+e^-} / d^3 x d^3 p$ at $\mathbf{p} = 0$ for the Sauter pulse. The diagonal dashed lines display loci of constant Keldysh parameters $\gamma = \frac{E_0}{m\tau}$. In the tunneling regime, $\gamma < 1$.

allow to address such an issue. Instead, we exhibit in Fig. 1 an example of an asymptotic photon spectrum for parameters E_0 and τ in the subcritical region, $E_0 < E_c$, $\tau > 1/m$. The individual contributions $(\int_{-\infty}^{-t_m} + \int_{t_m}^{\infty}) dt$ and $\int_{-t_m}^{t_m} dt$ to the coefficient (2) are separately displayed as a function of k_\perp (the component of \mathbf{k} perpendicular to $\mathbf{E} = (0, 0, E(t))$) at $k_\parallel = 0$ (the component of \mathbf{k} parallel to \mathbf{E} ; the full k_\perp - k_\parallel distribution is exhibited in the inset as a contour plot). Clearly visible are (i) the $1/\omega^3$ shape of the soft-photon distribution and (ii) the onset of the exponential decline of hard photons. In the optical-UV range, e.g. $\omega \sim 10^{-5}m$, we see a large phase-space occupancy of $f_\gamma = 10^5$. (In the spirit of the infrared catastrophe, the number of unobservably soft photons diverges logarithmically, while the energy emitted per unit volume remains finite.)

Figure 2 exhibits the photon numbers at $\omega = 10^{-5}m$ normalized to the residual e^+e^- pair number at $\mathbf{p} = 0$. Remarkably w.r.t. an experimental verification, the soft-photon numbers exceed by far the residual pair numbers¹ in the displayed patch of parameter space, e.g. $f_\gamma(\omega = 10^{-5}m)/f_{e^+e^-}(\mathbf{p} = 0) = 3.2 \times 10^8$ at $E_0 = 0.2E_c$ and $m\tau = 2$. (Due to the ω^{-3} scaling of f_γ for $\omega < 0.1m$, one can deduce from Fig. 2 the distribution of other soft-photon frequencies.) While encouraging for a detection

of the Schwinger process by a secondary probe, we see a monotonous reduction of the soft photon number relative to the pair number upon decreasing values of E_0 , when keeping the dynamical time scale τ fixed. However, extrapolating results of Fig. 2 to the regime of the Nuclear Physics pillar of the Extreme Light Initiative (ELI-NP)[28], $E_0 = 10^{-3}E_c$, $\tau = 5 \times 10^5/m$ [14], the ratio $f_\gamma(\omega = 10^{-5}m)/f_{e^+e^-}(\mathbf{p} = 0)$ becomes favourably 10^4 since both E_0 and τ are diminished. The employed values of E_0 and τ are deduced from the two-10 PW laser configuration as core of ELI-NP which is, according to the delivery plan (cf. [28]), envisaged to become operational in 2018. To extrapolate we exploit the apparent relation $\log f_\gamma = a \log E_0/E_c + b \log m\tau + c$ valid for small Keldysh parameters $\gamma \ll 1$. Therefore, real photons in the optical range, together with their nearly isotropic radiation pattern (see inset of Fig. 1) are identified as promising signature of the Schwinger effect. Their yield can be enhanced further by multi-scale field configurations.

2. Superposition of fields with different time scales

The superposition of a strong, slowly varying field with a weaker, fast-varying field is known to yield a residual pair number which can considerably exceed the residual pair number of each field alone – this is the dynamically assisted Schwinger effect [29] or assisted dynamical Schwinger effect [15]. Reference [17] states in more general terms that an increasing time-like inhomogeneity of a background field enhances the pair production. Figure 3 unravels an analog effect for the photons when considering the field model

$$E(t) = E_1 / \cosh^2(t/\tau) + E_2 / \cosh^2(Nt/\tau). \quad (3)$$

Being aware of the rather schematic character of the Sauter pulses employed above, we include here a field model which may be realized in the anti-nodes of pairwise counter propagating linearly polarized (laser) photon beams resulting in a purely electric background field $E(t)$ with potential $A(t)$ when ignoring the magnetic field components and the spatial inhomogeneity outside the anti-nodes. To be specific, our field model is

$$E(t) = K(t)\{E_1 \sin(t/\tau) + E_2 \sin(Nt/\tau)\}, \quad (4)$$

where $K(t)$ is a C^∞ smooth envelope function in [14]. In both cases, the Sauter pulse (3) and the model (4), the increased temporal inhomogeneity amplifies significantly (about four orders of magnitude in Fig. 3) the resulting asymptotic photon number. Whether other suitable field combinations enhance additionally the discovery potential of the Schwinger effect by a secondary probe needs more realistic modelling, including the back reaction. Similar to the Sauter pulse (cf. inset in Fig. 1) the emission is nearly isotropic, thus providing favorable observation conditions perpendicular to the background field(s) and their generating (laser) beams.

¹ Reference [27] provides an important example of particles in an intense external field which emit also multiple photons – even hard ones.

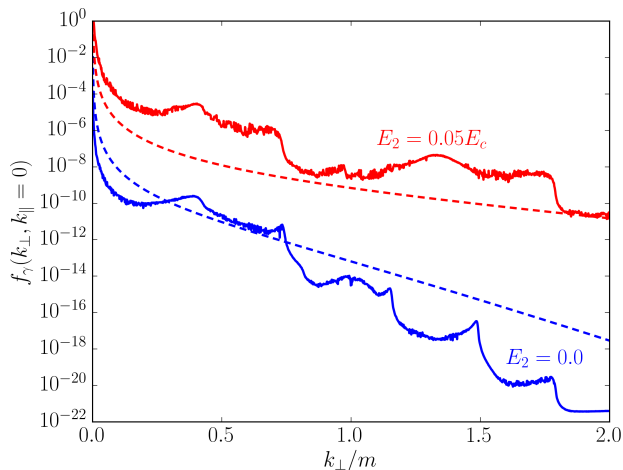


Figure 3. Asymptotic photon phase-space occupancy $f_\gamma(\mathbf{k})$ as a function of k_\perp at $k_\parallel = 0$ for the superposition (3) of Sauter pulses (dashed curves) and an oscillating field according to (4) (solid curves) with an envelope $K(t)$ according to [14] (flat-top interval $50 \cdot 2\pi \cdot \tau$ and (de)ramping time(s) $5 \cdot 2\pi \cdot \tau$). Parameters are $E_1 = 0.1E_c$, $\tau = 2/m$ and (i) $E_2 = 0$ (lower blue curves) and (ii) $E_2 = 0.05E_c$ and $N = 4$ (upper red curves). Note the exponential shape for hard photons with $\omega > 0.5m$ created in the Sauter pulse.

IV. SUMMARY

We consider in leading order the photon emission accompanying the process of shaking real electron-positron

pairs off the vacuum by the time-limited action of an external (spatially homogeneous) electric field. In contrast to photon emission at all wavelengths off a plasma at nonzero temperature (may it be an electron-positron plasma or a quark-gluon plasma), where rates are accessible in various formalisms, the non-perturbative character of pair creation due to the dynamical Schwinger process restricts us to the consideration of the final state occupancies, both of e^+e^- -pairs and photons. Nevertheless, the found photon spectra uncover all wavelengths too. Soft photons in the optical regime are produced amass and their abundancies can even exceed the abundancy of e^+e^- pairs in the sub critical region. Such a feature provides a promising signal of the Schwinger process and overcomes the unfavorably small number of residual e^+e^- pairs. The non linear amplification of the final photon yield by the superposition of two fields with different scales is for photons similar to the known effect in the residual pair sector, thus further enhancing the discovery potential of the secondary photon probe which should be exploited at ELI-NP.

Acknowledgements: The authors gratefully acknowledge inspiring discussions with H. Gies, F. Karbstein, R. Alkofer, D. B. Blaschke and C. Greiner. Many thanks go to S. Smolyansky and A. Panferov for common work on the plain Schwinger process. The fruitful collaboration with R. Sauerbrey and T. E. Cowan within the HIBEF project lead to the present investigation.

Appendix A: The photon spectrum

The differential spectrum of single photons with momenta \mathbf{k} summed over polarizations λ at time instant t is defined by

$$\frac{d^3N_\gamma(t, \mathbf{k})}{d^3k} = \frac{1}{(2\pi)^3} \sum_\lambda \langle 0 | a_{\lambda,H}^\dagger(t, \mathbf{k}) a_{\lambda,H}(t, \mathbf{k}) | 0 \rangle \quad (\text{A1})$$

where $a_{\lambda,H}^\dagger/a_{\lambda,H}$ are corresponding creation/annihilation operators in the Heisenberg picture (H); in the interaction picture (I)² the photon field operator $\mathcal{A}_I^\mu(t, \mathbf{x})$ obeys the general decomposition

$$\mathcal{A}_I^\mu(t, \mathbf{x}) = \int \frac{d^3k}{\sqrt{2\omega}(2\pi)^3} \sum_\lambda \left[a_\lambda(\mathbf{k}) \varepsilon_\lambda^\mu(\mathbf{k}) e^{-ikx} + a_\lambda^\dagger(\mathbf{k}) \varepsilon_\lambda^{\mu*}(\mathbf{k}) e^{ikx} \right] \quad (\text{A2})$$

with $k^2 = \omega^2 - \mathbf{k}^2 = 0$ and $\varepsilon_\lambda^\mu(\mathbf{k})k_\mu = 0$, pointing to on-shell photons propagating on the light cone with two transverse polarizations (μ is a Lorentz index). The vacuum definition employed in (A1) reads $a_\lambda(\mathbf{k})|0\rangle = 0$ w.r.t. the photons; the photons in turn are sourced by a Dirac current operator driving the photon dynamics according to the wave equation

$$\partial^2 \mathcal{A}_H^\mu(t, \mathbf{x}) = e j_H^\mu(t, \mathbf{x}) \quad (\text{A3})$$

² For the reader's convenience we recall the transformation of operators O between the various pictures. The Heisenberg picture (H) follows from (i) the Schrödinger picture (S) by $O_H(t) = U^\dagger(t, t_0) O_S(t_0) U(t, t_0)$ or from (ii) the interaction picture (I) by $O_H(t) = U_{\text{int}}^\dagger(t, t_0) O_I(t) U_{\text{int}}(t, t_0)$, and

(I) from (iii) (S) by $O_I(t) = U_0^\dagger(t, t_0) O_S(t_0) U_0(t, t_0)$; (iii) causes $a_{\lambda,I}(t, \mathbf{k}) = U_0^\dagger(t, t_0) a_\lambda(\mathbf{k}) e^{-i\omega t_0} U_0(t, t_0) = a_\lambda(\mathbf{k}) e^{-i\omega t}$ and (ii) causes $a_{\lambda,H}(t, \mathbf{k}) = U_{\text{int}}^\dagger(t, t_0) a_{\lambda,I}(t, \mathbf{k}) U_{\text{int}}(t, t_0) = U_{\text{int}}^\dagger(t, t_0) a_\lambda(\mathbf{k}) e^{-i\omega t} U_{\text{int}}(t, t_0)$.

with gauge conditions $\mathcal{A}_H^0 = 0$, $\nabla \cdot \mathcal{A}_H = 0$ which are equivalent to $\epsilon_\lambda^0(\mathbf{k}) = 0$ and $\epsilon_\lambda(\mathbf{k}) \cdot \mathbf{k} = 0$. Equation (A3) is solved by a suitable unitary operator $U_{\text{int}}(t, t_0)$ via $\mathcal{A}_H(t, \mathbf{x}) = U_{\text{int}}^\dagger(t, t_0) \mathcal{A}_I(t, \mathbf{x}) U_{\text{int}}(t, t_0)$ and $j_H^\mu(t, \mathbf{x}) = U_{\text{int}}^\dagger(t, t_0) j_I^\mu(\mathbf{x}) U_{\text{int}}(t, t_0)$, where the current operator j_I^μ is constrained to $j_I^\mu(t, \mathbf{x}) = :\bar{\Psi}_I(t, \mathbf{x}) \gamma^\mu \Psi_I(t, \mathbf{x}) :$. The notation $:\cdots:$ stands for normal ordering w.r.t. the vacuum $|0\rangle$ and the operators c_r and d_r introduced below in (A4). This constraint omits the vacuum expectation value of $\bar{\Psi}_I \gamma^\mu \Psi_I$, which is non-zero in a background field and creates a c-number component of \mathcal{A}_H which counteracts to the externally applied background field A . We neglect that backreaction (see e.g. [30]) since we are interested here in the quantum part of the radiation field, which is henceforth dealt with in the probe limit.

The needed Dirac wave operator can be decomposed in the interaction picture as

$$\Psi_I(t, \mathbf{x}) = \int \frac{d^3 p}{(2\pi)^3} \sum_r \left[c_r(\mathbf{p}) u_r(t, \mathbf{p}, \mathbf{x}) + d_r^\dagger(\mathbf{p}) v_r(t, \mathbf{p}, \mathbf{x}) \right] \quad (\text{A4})$$

which extends the vacuum definition by $c_r|0\rangle = d_r|0\rangle = 0$; c_r and d_r^\dagger carry the operator character and u_r and v_r the bispinor structure.

In the interaction picture, the fermion dynamics obeys the Dirac equation

$$\{i\gamma^\mu(\partial_\mu + ieA_\mu) + m\} \Psi_I(t, \mathbf{x}) = 0. \quad (\text{A5})$$

We assume our purely electric background field A_μ to be spatially homogeneous, but time dependent, which allows to split off the \mathbf{x} dependence of the wave functions by replacing $u_r(t, \mathbf{p}, \mathbf{x}) \rightarrow u_r(t, \mathbf{p}) e^{i\mathbf{p}\mathbf{x}}$ and $v_r(t, \mathbf{p}, \mathbf{x}) \rightarrow v_r(t, \mathbf{p}) e^{-i\mathbf{p}\mathbf{x}}$ in (A4) with

$$\{i\gamma^0 \partial_t - \boldsymbol{\gamma}(\mathbf{p} - e\mathbf{A}(t)) - m\} u_r(t, \mathbf{p}) = 0 \quad (\text{A5}')$$

(same for $v_r(t, -\mathbf{p})$) and initial conditions $u_r(t \rightarrow -\infty, \mathbf{p}) \propto u_r(\mathbf{p}) e^{-i\sqrt{m^2 + \mathbf{p}^2} t}$ and $v_r(t \rightarrow \infty, \mathbf{p}) \propto v_r(\mathbf{p}) e^{i\sqrt{m^2 + \mathbf{p}^2} t}$.

With these ingredients we evaluate (A1) by employing $a_{\lambda, H}(t, \mathbf{k}) = U_{\text{int}}^\dagger(t, t_0) a_{\lambda, I}(t, \mathbf{k}) U_{\text{int}}(t, t_0)$ with Dyson's series

$$U_{\text{int}}(t, t_0) = \text{Texp} \left(-i \int_{t_0}^t dt' f_\varepsilon(t') H_{\text{int}, I}(t') \right) \cong 1 - i \int_{t_0}^t dt' f_\varepsilon(t') H_{\text{int}, I}(t') + \mathcal{O}(e^2), \quad (\text{A6})$$

where T means the time ordering operation and $f_\varepsilon(t) = e^{-\varepsilon|t|}$ is used to adiabatically turn the interaction on and off. At the end of our calculation, we let $\varepsilon \rightarrow 0$. We restrict ourselves to the leading-order non-trivial term of (A6) and utilize³

$$H_{\text{int}, I}(t) = e \int d^3 x \mathcal{A}_I^\mu(t, \mathbf{x}) j_{I, \mu}(t, \mathbf{x}). \quad (\text{A7})$$

This yields for $a_{\lambda, H}$ up to order $\mathcal{O}(e^3)$

$$\begin{aligned} a_{\lambda, H}(t, \mathbf{k}) &= \left[1 + i \int_{t_0}^t dt' H_{\text{int}, I}(t') \right] a_{\lambda, I}(t, \mathbf{k}) \left[1 - i \int_{t_0}^t dt' H_{\text{int}, I}(t') \right] \\ &= \left[a_\lambda(\mathbf{k}) + i \int_{t_0}^t dt' \int d^3 x : \bar{\Psi}_I(t', \mathbf{x}) [e\gamma_\mu \mathcal{A}_I^\mu(t', \mathbf{x}), a_\lambda(\mathbf{k})] \Psi_I(t', \mathbf{x}) : \right] e^{-i\omega t} \\ &= \left[a_\lambda(\mathbf{k}) - i \frac{e\varepsilon_\lambda^{*\mu}(\mathbf{k})}{\sqrt{2\omega}} \int_{t_0}^t dt' \int d^3 x : \bar{\Psi}_I(t', \mathbf{x}) \gamma_\mu \Psi_I(t', \mathbf{x}) : e^{ikx'} \right] e^{-i\omega t}. \end{aligned} \quad (\text{A8})$$

Insertion into (A1) lets us arrive at

$$\begin{aligned} \frac{d^3 N_\gamma(t)}{d^3 k} &= \frac{e^2}{(2\pi)^6} \frac{1}{2\omega} \sum_\lambda \varepsilon_\lambda^\mu(\mathbf{k}) \varepsilon_\lambda^{*\nu}(\mathbf{k}) \int_{t_0}^t dt_1 \int_{t_0}^t dt_2 \int d^3 x_1 \int d^3 x_2 f_\varepsilon(t_1) f_\varepsilon(t_2) \\ &\quad \times \langle 0 | : \bar{\Psi}_I(t_1, \mathbf{x}_1) \gamma_\mu \Psi_I(t_1, \mathbf{x}_1) : : \bar{\Psi}_I(t_2, \mathbf{x}_2) \gamma_\nu \Psi_I(t_2, \mathbf{x}_2) : | 0 \rangle e^{-ik(x_1 - x_2)} \\ &= \frac{e^2}{(2\pi)^6} \frac{1}{2\omega} \sum_{\lambda, r, s} \varepsilon_\lambda^\mu(\mathbf{k}) \varepsilon_\lambda^{*\nu}(\mathbf{k}) \int d^3 x \int \frac{d^3 p}{(2\pi)^3} \int_{t_0}^t dt_1 \bar{v}_r(t_1, -\mathbf{p}) \gamma_\mu u_s(t_1, \mathbf{p} - \mathbf{k}) f_\varepsilon(t_1) e^{-i\omega t_1} \\ &\quad \times \int_{t_0}^t dt_2 \bar{u}_s(t_2, \mathbf{p} - \mathbf{k}) \gamma_\nu v_r(t_2, -\mathbf{p}) f_\varepsilon(t_2) e^{-i\omega t_2}. \end{aligned} \quad (\text{A9})$$

³ We note the relations $H_I = H_{0, I} + H_{\text{int}, I}$ with $H_{0, I} = \int d^3 x \{ \bar{\Psi}_I [\boldsymbol{\gamma}(-i\nabla - e\mathbf{A} + m) \Psi_I + \frac{1}{2} [\dot{\mathcal{A}}_I^2 + (\nabla \times \mathcal{A}_I)^2] \}$.

Note that $d^3 N_\gamma(t = t_0)/d^3 k = 0$. We define the dimensionless photon phase-space occupation number $f_\gamma(\mathbf{k}) = d^6 N_\gamma(t \rightarrow \infty, \mathbf{k})/d^3 x d^3 k$ and get the basic equations (1,2). We emphasize again that (1,2) are independent of a special ‘‘driver’’ of the dynamics of $u_r(t)$ and $v_r(t)$, e.g. omitting in the Dirac equation the external field A and allowing instead for a dynamical effective mass $m(t)$, steered by the coupling to another background, one recovers the results of [31], albeit noted here in a different form.

Appendix B: Soft photons

To study the soft photon limit one may split the time integral in Eq. (2) in the main text according to $\int_{-\infty}^{\infty} dt = \int_{-\infty}^{-t_m} dt + \int_{-t_m}^{t_m} dt + \int_{t_m}^{\infty} dt$, where t_m stands for a matching scale with the meaning that the background field \mathbf{A} induces a noticeable dynamics of the fermion field only within $-t_m \dots t_m$, that is $\dot{\mathbf{A}}(t \leq t_m) = \dot{\mathbf{A}}(t \geq t_m) = 0$. We set $\mathbf{A}(t \leq t_m) = 0$ and $\mathbf{A}(t \geq t_m) = \mathbf{A}_\infty$ and elaborate $\lim_{\omega \rightarrow 0} C_{rs\mu}$. Employing

$$\begin{aligned} u_r(t \leq -t_m, \mathbf{p}) &= e^{-i\Omega(\mathbf{p})(t+t_m)} u_r(\mathbf{p}), \\ v_r(t \leq -t_m, -\mathbf{p}) &= e^{i\Omega(\mathbf{p})(t+t_m)} v_r(-\mathbf{p}), \\ u_r(t \geq t_m, \mathbf{p}) &= \alpha(t_m, \mathbf{p}) e^{-i\Theta(t_m, \mathbf{p})} e^{-i\Omega(\mathbf{P}_\infty)(t-t_m)} u_r(\mathbf{P}_\infty) \\ &\quad + \beta(t_m, \mathbf{p}) e^{i\Theta(t_m, \mathbf{p})} e^{i\Omega(\mathbf{P}_\infty)(t-t_m)} v_r(-\mathbf{P}_\infty), \\ v_r(t \geq t_m, -\mathbf{p}) &= -\beta^*(t_m, \mathbf{p}) e^{-i\Theta(t_m, \mathbf{p})} e^{-i\Omega(\mathbf{P}_\infty)(t-t_m)} u_r(\mathbf{P}_\infty) \\ &\quad + \alpha^*(t_m, \mathbf{p}) e^{i\Theta(t_m, \mathbf{p})} e^{i\Omega(\mathbf{P}_\infty)(t-t_m)} v_r(-\mathbf{P}_\infty) \end{aligned} \quad (\text{B1})$$

with $\Omega(\mathbf{p})^2 = m^2 + \mathbf{p}^2$, $\Theta(t, \mathbf{p}) = \int_{-t_m}^t dt' \Omega(\mathbf{p} - e\mathbf{A}(t'))$ and $\mathbf{P}_\infty = \mathbf{p} - e\mathbf{A}_\infty$ from a Bogoliubov transformation (see below) results in the leading order term

$$\lim_{\omega \rightarrow 0} C_{rs\mu}(\mathbf{p}, \mathbf{k}) = -i\alpha(t_m, \mathbf{p})\beta(t_m, \mathbf{p}) \left[\frac{\bar{v}_r(-\mathbf{P}_\infty)\gamma_\mu v_s(-\mathbf{P}_\infty)}{\omega + \frac{\mathbf{P}_\infty \mathbf{k}}{\Omega(\mathbf{P}_\infty)}} + \frac{\bar{u}_r(\mathbf{P}_\infty)\gamma_\mu u_s(\mathbf{P}_\infty)}{\omega - \frac{\mathbf{P}_\infty \mathbf{k}}{\Omega(\mathbf{P}_\infty)}} \right] + \mathcal{O}(\omega^0). \quad (\text{B2})$$

The relation (B2) shows that $\lim_{\omega \rightarrow 0} C \propto 1/\omega$ for a non-zero Bogoliubov coefficient $\beta(t_m, \mathbf{p})$, while $\lim_{\omega \rightarrow 0} C$ (labels and index suppressed) remains finite for $\beta(t_m, \mathbf{p}) = 0$ due to the $\mathcal{O}(\omega^0)$ term. As a consequence, in the former case $f_\gamma \propto 1/\omega^3$, while in the latter case $f_\gamma \propto 1/\omega$. $\beta(t_m, \mathbf{p}) \neq 0$ implies an asymptotic pair density $N_{e^+e^-} \propto |\beta|^2$, that is a specific soft photon spectrum accompanying a non-zero residual pair number. In the terminology of [31], these contributions refer to bremsstrahlung terms. We emphasize here the mere use of well defined *in*- and *out*-states and employed correspondingly a time-limited action of the background field.

In deriving (B1,B2) we use the Bogoliubov transformation to solve the Dirac equation. Introducing the Hamiltonian $h(\mathbf{p}) = \gamma^0(\mathbf{p}\boldsymbol{\gamma} + m)$ in first quantization and the canonical momentum $\mathbf{P}(t) = \mathbf{p} - e\mathbf{A}(t)$ the governing equations for u_r and v_r read

$$\{i\partial_t - h(\mathbf{P}(t))\} u_r(t, \mathbf{p}) = 0, \quad \{i\partial_t - h(\mathbf{P}(t))\} v_r(t, -\mathbf{p}) = 0, \quad (\text{B3})$$

$$u_r(-t_m, \mathbf{p}) = u_r(\mathbf{p}), \quad v_r(-t_m, -\mathbf{p}) = v_r(-\mathbf{p}). \quad (\text{B4})$$

We chose our initial condition at $t = -t_m$. Since \mathbf{A} points along the z -direction, $\mathbf{A}(t) = A(t)\mathbf{e}_z$, we use an ansatz for $u_r(\mathbf{p})$ and $v_r(-\mathbf{p})$

$$u_r(\mathbf{p}) = \frac{\Omega(\mathbf{p}) + h(\mathbf{p})}{\sqrt{2\Omega(\mathbf{p})(\Omega(\mathbf{p}) - p_z)}} R_r, \quad v_r(-\mathbf{p}) = \frac{-\Omega(\mathbf{p}) + h(\mathbf{p})}{\sqrt{2\Omega(\mathbf{p})(\Omega(\mathbf{p}) + p_z)}} R_r, \quad (\text{B5})$$

where R_r denote two spinors ($r = 1, 2$) that are eigenvectors of $\gamma^0\boldsymbol{\gamma}^3$ with the eigenvalue -1 . With this ansatz, u_r and v_r are orthogonal and have the following convenient properties:

$$h(\mathbf{p})u_r(\mathbf{p}) = \Omega(\mathbf{p})u_r(\mathbf{p}), \quad h(\mathbf{p})v_r(-\mathbf{p}) = -\Omega(\mathbf{p})v_r(-\mathbf{p}), \quad (\text{B6})$$

$$\partial_t u_r(\mathbf{P}(t)) = \frac{eE(t)\epsilon_\perp}{2\Omega(\mathbf{P}(t))^2} v_r(-\mathbf{P}(t)), \quad \partial_t v_r(-\mathbf{P}(t)) = -\frac{eE(t)\epsilon_\perp}{2\Omega(\mathbf{P}(t))^2} u_r(\mathbf{P}(t)), \quad (\text{B7})$$

with $E(t) = -\dot{A}(t)$ the electric field and $\epsilon_{\perp} = \sqrt{m^2 + p_x^2 + p_y^2}$ the transverse energy. With these base spinors, the full solutions $u_r(t, \mathbf{p})$ and $v_r(t, -\mathbf{p})$ are sought in the form

$$u_r(t, \mathbf{p}) = \alpha(t, \mathbf{p})e^{-i\Theta(t, \mathbf{p})}u_r(\mathbf{P}(t)) + \beta(t, \mathbf{p})e^{i\Theta(t, \mathbf{p})}v_r(-\mathbf{P}(t)), \quad (\text{B8})$$

$$v_r(t, -\mathbf{p}) = -\beta^*(t, \mathbf{p})e^{-i\Theta(t, \mathbf{p})}u_r(\mathbf{P}(t)) + \alpha^*(t, \mathbf{p})e^{i\Theta(t, \mathbf{p})}v_r(-\mathbf{P}(t)), \quad (\text{B9})$$

which directly lead to (B1). Plugging (B8) together with (B6) and (B7) into (B3) leads to the following coupled equations for α and β (the ansatz (B9) leads to the same equations):

$$\dot{\alpha}(t, \mathbf{p}) = \frac{eE(t)\epsilon_{\perp}}{2\Omega(\mathbf{P}(t))^2}e^{2i\Theta(t, \mathbf{p})}\beta(t, \mathbf{p}), \quad (\text{B10})$$

$$\dot{\beta}(t, \mathbf{p}) = -\frac{eE(t)\epsilon_{\perp}}{2\Omega(\mathbf{P}(t))^2}e^{-2i\Theta(t, \mathbf{p})}\alpha(t, \mathbf{p}), \quad (\text{B11})$$

which are solved numerically. The initial conditions (B4) translate to $\alpha(t = -t_m, \mathbf{p}) = 1$ and $\beta(t = -t_m, \mathbf{p}) = 0$. The meaning of α and β comes from $N_{e^+e^-}(t \rightarrow \infty, \mathbf{p}) = 2|\beta(t \rightarrow \infty, \mathbf{p})|^2$, i.e. β determines directly the number of pairs created by the electric background field.

-
- [1] J. Schwinger, Phys. Rev. **82**, 664 (1951).
 - [2] F. Sauter, Z. Phys. **69**, 742 (1931).
 - [3] F. Gelis and N. Tanji, Prog. Part. Nucl. Phys. **87**, 1 (2016).
 - [4] S. W. Hawking, Nature **248**, 30 (1974).
 - [5] G. W. Gibbons and S. W. Hawking, Phys. Rev. D **15**, 2738 (1977).
 - [6] W. G. Unruh, Phys. Rev. D **14**, 870 (1976).
 - [7] L. Parker, Phys. Rev. Lett. **21**, 562 (1968); Phys. Rev. **183**, 1057 (1969); Phys. Rev. D **3**, 346 (1971).
 - [8] A. Casher, H. Neuberger, and S. Nussinov, Phys. Rev. D **20**, 179 (1979).
 - [9] A. Di Piazza, C. Müller, K. Z. Hatsagortsyan, and C. H. Keitel, Rev. Mod. Phys. **84**, 1177 (2012).
 - [10] M. Orthaber, F. Hebenstreit, and R. Alkofer, Phys. Lett. B **698**, 80 (2011).
 - [11] C. Kohlfürst, M. Mitter, G. von Winckel, F. Hebenstreit, and R. Alkofer, Phys. Rev. D **88**, 045028 (2013).
 - [12] F. Hebenstreit and F. Fillion-Gourdeau, Phys. Lett. B **739**, 189 (2014).
 - [13] I. Akal, S. Villalba-Chávez, and C. Müller, Phys. Rev. D **90**, 113004 (2014).
 - [14] A. Otto, D. Seipt, D. Blaschke, B. Kämpfer, and S. A. Smolyansky, Phys. Lett. B **740**, 335 (2015).
 - [15] A. Otto, D. Seipt, D. B. Blaschke, S. A. Smolyansky, and B. Kämpfer, Phys. Rev. D **91**, 105018 (2015).
 - [16] A. Ringwald, Phys. Lett. B **510**, 107 (2001).
 - [17] A. Ilderton, G. Torgrimsson, and J. Wårdh, Phys. Rev. D **92**, 065001 (2015).
 - [18] H. Gies and G. Torgrimsson, Phys. Rev. Lett. **116**, 090406 (2016).
 - [19] L. McLerran and T. Toimela, Phys. Rev. D **31**, 545 (1985).
 - [20] C. Shen, J.-F. Paquet, U. Heinz, and C. Gale, Phys. Rev. C **91**, 014908 (2015).
 - [21] F. Karbstein and R. Shaisultanov, Phys. Rev. D **91**, 113002 (2015).
 - [22] D. B. Blaschke, A. V. Prozorkevich, G. Röpke, C. D. Roberts, S. M. Schmidt, D. S. Shkirmanov, and S. A. Smolyansky, Eur. Phys. J. D **55**, 341 (2009).
 - [23] M. Kuchiev and J. Ingham, (2015), arXiv:1511.06806.
 - [24] D. Blaschke, S. M. Schmidt, S. A. Smolyansky, and A. V. Tarakanov, Phys. Part. Nucl. **41**, 1004 (2010).
 - [25] A. Otto, T. Nusch, D. Seipt, B. Kämpfer, D. Blaschke, A. D. Panferov, S. A. Smolyansky, and A. I. Titov, J. Plasma Phys. **82**, 655820301 (2016).
 - [26] A. D. Panferov, S. A. Smolyansky, A. Otto, B. Kämpfer, D. B. Blaschke, and L. Juchnowski, Eur. Phys. J. D **70**, 1 (2016).
 - [27] A. D. Piazza, K. Z. Hatsagortsyan, and C. H. Keitel, Phys. Rev. Lett. **105**, 220403 (2010).
 - [28] *ELI Nuclear Physics (ELI-NP)*, www.eli-np.ro.
 - [29] R. Schützhold, H. Gies, and G. Dunne, Phys. Rev. Lett. **101**, 130404 (2008).
 - [30] J. C. R. Bloch, V. A. Mizerny, A. V. Prozorkevich, C. D. Roberts, S. M. Schmidt, S. A. Smolyansky, and D. V. Vinnik, Phys. Rev. D **60**, 116011 (1999).
 - [31] F. Michler, H. van Hees, D. D. Dietrich, and C. Greiner, Phys. Rev. D **89**, 116018 (2014).